The applicability of cellulose -Tara gum composite hydrogels as dye capture adsorbents

Diego Gomez-Maldonado, [a] Silvia Ponce, [b] Maria S. Peresin [a1]*

[a] Forest Products Development Center, College of Forestry, Wildlife and Environment, Auburn University, 602 Duncan Dr., Auburn, Alabama 36830, United States

[b] Applied Nanomaterials Research Group, Institute of Scientific Research IDIC, Universidad de Lima, Av. Javier Prado Este 4600 Surco, Lima 33, Peru

Highlights

- Bead-shaped hydrogels can be produced by regeneration of cellulose nanofibrils instead of dissolving pulp.
- The solid content of the beads was substituted by up to 50% with Tara gum.
- 40% Tara gum allowed us to generate structurally sound beads with a lower density.
- The presence of Tara gum in the fibers of the beads improved the adsorption capacity of Methylene Blue by 39.6%.
- The maximum adsorption capability of the 40% substituted beads was 13.7 mg/g when isotherm data was fitted into a Langmuir model.

[*] Maria Soledad Peresin, Ph.D.
Email address: soledad.peresin@auburn.edu

Abstract

There is a growing interest in using naturally derived materials to generate adsorbent materials that can improve water quality by removing industrially derived pollutants such as dyes. In this work, composite beads were prepared from wood-based cellulose nanofibrils (CNF) and Tara gum (TG) by their co-dissolution in urea/sodium hydroxide alkaline media followed by co-regeneration in acidic media. The obtained beads were characterized by Fourier transformed infrared with attenuated total reflectance (FTIR-ATR), X-ray diffraction (XRD), thermogravimetric analysis (TGA), elemental analysis (EA), and scanning electron microscopy (SEM), while the dye adsorption capacity was followed by UV-vis spectroscopy. The results showed that a 40% substitution of the CNF with TG resulted in lightweight beads with 54% less solid content that maintained similar dimensions. These beads were tested for methylene blue (MB) adsorption at varying sorbent and pollutant concentrations. Methylene blue was selected as it is a common dye used as a redox indicator for tissue staining, dairy testing, microbiology, and in the textile and leather industries. Overall, the TG-CNF composite beads showed improved performance on dye adsorption, with 39.6% more capture when compared to the neat cellulose beads. The maximum adsorption capacity was calculated as 13.7 mg/g, utilizing an adsorption isotherm (2-15 ppm) fitted into the Langmuir model.

Keywords: agrowaste valorization; cellulose II; nanocellulose; methylene blue; water remediation.

1. Introduction

Some of the most common pollutants in wastewater are dyes (Cai et al. 2017). Multiple modern economic activities depend on these, such as the textile and leather tanning industries, food technology, pulp and paper manufacturers, agricultural research, photoelectrochemical cells, and cosmetic applications, among others (Forgacs et al. 2004; Rahimian and Zarinabadi 2020). Furthermore, as most of them are water soluble, an effective recovery or treatment is challenging, turning them into a hazard for human health because of their carcinogenesis (Shore 2002; Lang 2009; Gürses et al. 2016). Likewise, the presence of these dyes in industrial effluents has a negative impact on both flora and fauna, even when present at low concentrations.

Several technologies are used to remove these pollutants, such as flowing the contaminated water through activated sludges, photocatalysis, chemical oxidation, and microbial or enzymatic degradation (Forgacs et al. 2004). However, most of them have shown less performance when compared to remediation by adsorption. Generally, the most widely utilized adsorbent is activated charcoal, which has shown a high adsorption capacity of organic species (Mahmoud et al. 2013; Cai et al. 2017). Nevertheless, it is very expensive, difficult to recover, and it can become unstable during reuse as its physical integrity decreases over time (Mokhtar et al. 2020).

Thus, the use of low cost and environmentally friendly materials as adsorbents in water remediation is a priority, also considering that few to no royalties are generated during the wastewater treatment process. Lignocellulosic materials derived from biomass and agroforest residues are an attractive alternative to develop adsorbent materials. Of particular interest in this work, is the underutilized Tara gum.

Tara (*Caesalpinia spinosa (Molina) Kuntze*) is a native shrub from Peru, from which products such as Tara gum (TG), Tara powder, and tannins can be obtained. Tara gum is used worldwide in the food industry for its capacity to change the rheological properties of products such as ice cream, creamery products, and other milk derivatives. Tara gum is obtained by grinding the seeds after they are separated from the pods, resulting in a relatively inexpensive material that is naturally biocompatible (Wu et al. 2015).

Tara gum traditionally has a lower molecular weight (Prado et al. 2005) compared to other commonly used polysaccharides like cellulose and chitosan, which presents a challenge for standalone use in product development. Conversely, cellulose is the most abundant natural polymer as it is widely present in wood, plants, and algae and can also be synthesized as a byproduct by some bacteria and animals (Klemm et al. 2011; Jonoobi et al. 2015). Cellulose has gained attention in developing a wide variety of dimensionally stable hydrogels and aerogels with high surface areas and low densities, which are great candidates for their use in water purification and capture of pollutants.(Qiu and Hu 2013; Wang et al. 2013; Zhang et al. 2013; Long et al. 2018). Composite materials of cellulose and Tara gum have been previously described (Ma and Wang 2016; Ma et al. 2016; Ponce et al. 2020), demonstrating the potential of combining these two natural polymers.

When comparing the different hydrogels achievable, the spherical shape of beads is beneficial for water remediation as it can decrease the backpressure under flow conditions (Ruan et al. 2018). Furthermore, bead structures made of cellulose have been applied in other processes like controlled drug release (Trygg et al. 2015), chromatography and catalytic packing for columns (Wang et al. 2007; Luan et al. 2021),

and for noble metal adsorption (Ruan et al. 2016). However, to produce these cellulose beads, pretreatment of dissolving pulp with acid ethanol is required (Trygg and Fardim 2011; Gomez-Maldonado et al. 2021a) or premodification of high molecular cellulose like cotton linters (Trygg et al. 2014; Luan et al. 2021). Furthermore, concentrations of 4% or above are the required to have stable bead structures (Trygg et al. 2013).

This work demonstrates that hydrogel beads can be generated using 1.4% alkaline solutions when starting from nanofibrillated cellulose (CNF) and that they are capable of dye removal. Additionally, beads were generated when combined with Tara gum at varying ratios, improving its removal capacity performance. Their ability to adsorb methylene blue (MB) was assessed by in vitro tests varying the dyes and sorbents concentrations and followed by UV-Vis spectroscopy. The obtained data was fitted into Langmuir and Freundlich models to calculate the maximum adsorption capacity and adsorption constants.

2. Experimental

2.1 Materials

Bleached cellulose nanofibrils (CNF, 1.91%, pH 6.3) were produced at the Forest Products Development Center (Auburn University, Auburn, AL) from bleached pulp obtained from mixed softwood, which was kindly provided by a North American mill. Tara gum (TG) dry powder was kindly provided by MASAC (Molinos Asociados SAC, Peru). Crystalized Urea was purchased from VWR (Radnor, Pennsylvania, U.S.).

NaOH pearls (97% purity) were purchased from ALFA AESAR (Ward Hill, Massachusetts, U.S). Methylene blue (MB) was purchased from Merck KGaA (Darmstadt, Germany). Ultrapure water was deionized and purified with a Thermo Scientific Barnstead nanopure system (18.2 mΩ cm). Unless specified, all the weights in this paper are expressed on oven dry basis.

2.2 Production of cellulose nanofibril (CNF)

The nanocellulose utilized in this work was produced as explained in the previous work (Gomez-Maldonado et al. 2021b) . Briefly, a 2% wt. pulp suspension was washed in acidic and alkaline conditions to eliminate any residual metals or other contaminants present on the pulp. Then, the neutralized pulp was passed 20 times in a Masuko super mass colloider (MKZA-10-15J); obtaining a suspension with a 2.8% consistency at a pH of 6.3.

2.3 Formation of the cellulose nanofibril/Tara gum beads

For the generation of the beads, the cellulose nanofibrils aqueous suspension was used as a starting material to generate a 12% Urea-7% NaOH solution; water, urea, and NaOH were added as needed to obtain a final solid content of 1.4% w/v. The nanocellulose suspension used for the solid content was modified to substitute 10, 30, 40, and 50% with dry Tara gum powder. The new solution was stirred at -10 °C for 1 h to allow the Tara gum to fully dissolve and for proper homogeneity. Once dissolved, the solution was added dropwise using a syringe needle 21G 100 (0.8192 mm outer

diameter) to a volumetric cylinder containing 2 M nitric acid to allow for the material regeneration. Finally, once formed, the beads were washed with repeated changes of fresh ultrapure water until a neutral pH was obtained.

2.4 Characterization

Solid content and size. A total of five beads were weighted in aluminum pans and dried in a convection oven at 105 °C overnight. The moisture content was then calculated according to equation (1). This measurement was done by triplicated, and average values were reported.

$$MC\ \% = \frac{mass_{wet} - mass_{dry}}{mass_{wet}} * 100\ \% \quad (1)$$

The average size was obtained after measuring the diameter of 10 beads using a caliper.

Fourier transformed infrared with attenuated total reflectance (FTIR-ATR). Freeze-dried samples were analyzed with a Perkin Elmer Spotlight 400 FT-IR Imaging System, equipped with an ATR accessory with diamond/ZnSe crystal. 128 scans with a 4 cm^{-1} resolution were collected and the data was processed with Spectrum 6 Spectroscopy Software (Massachusetts, US).

X-ray diffraction (XRD). Freeze-dried samples were ground into powder and analyzed using a RIGAKU Smartlab SE model equipped with Cu Kα irradiation (λ= 1.541 Å) at 40 kV and 50 mA to obtain the corresponding spectra. Measurements were performed at a scan speed of 0.1 sec/step from 10° to 60° θ/2θ, at 10°/min.

Elemental analysis (EA). The elemental analysis (CHNS/O) was performed in a Vario MICRO cube, Elementar, (Ronkonkoma, NY, U.S.) with the conditions set according to the ASTM D5373-02 method.

Thermogravimetric analysis (TGA). Freeze-dried samples were tested on aluminum pans in a TGA-50 Shimadzu Thermogravimetric Analyzer (Kyoto, Japan). Samples were tested in a temperature range from room temperature (25 °C) to 600 °C at a rate of 10 °C/min under a nitrogen atmosphere at a rate of 20 mL/min. The thermograms and their corresponding first derivative were recorded for each sample using the software TA-60WS (Kyoto, Japan). Measurements were done by duplicated, and average values were reported.

Scanning electron microscopy (SEM). Freeze-dried beads were placed on standard aluminum studs with carbon tape and sputtered with gold for 60 s in a Q150R ES sputter coating device (Hatfield, PA, U.S.). All the images were recorded using an intensity of 20 kW, with working distances between 6 and 8 mm in a Zeiss Evo 50VP scanning electron microscope.

2.5 Methylene Blue (MB) Adsorption

Dye removal capacity. For measuring the effect of the substitution of CNF with TG in the dye adsorption performance, 20 mL of methylene blue solution at a concentration of 15 mg/L was placed in 3 separate beakers. Five beads (8 wet mg) were added, aiming at minimizing instrumental error. Aliquots were extracted and analyzed in a Genesys 50 UV-Visible Spectrophotometer from Thermo Scientific (Waltham, MA U.S.) every

30 min for the first 5 h and then at 24 h. The wavelength of the test was λ=664 nm and the data collected was fitted into a standard curve ranging from 0 to 18 mg/L. Removal percentage of the dye from the solution was calculated according to equation 2:

$$\text{Dye removal \%} = \frac{[MB]_{intial} - [MB\}_{final}}{[MB\}_{initial}} * 100\ \% \quad (2)$$

The obtained data was fitted into the pseudo-first-order kinetic model (equation 3), and into the pseudo-second-order kinetic model (equation 4).

$$\mathrm{Ln}(q_e - q_t) = \mathrm{Ln}q_e - \frac{k_1 t}{2.303} \quad (3)$$

$$\frac{1}{q_t} = \frac{1}{k_2 q_e^2} + \frac{1}{q_e} t \quad (4)$$

where k_1 and k_2 are the rate constants, q_e is the adsorption on equilibrium and q_t is the adsorption in each time point sampled.

Adsorption isotherms. For constructing adsorption isotherms, 200 mg of wet beads were placed in 10 mL of methylene blue solutions with 2, 5, 8, 10 and 15-ppm and left under dark conditions at room temperature for 48 h before measuring the absorbance of the solutions. Meanwhile, isotherms at constant concentration were also investigated. To this end, the beads wet mass (0.1, 0.2, 0.3, 0.4, 0.5, 0.6, 0.7, and 0.8 g) were immersed in 10 mL of 15-ppm methylene blue solution, in the same conditions previously stated. All measurements were done by duplicate and averaged, Langmuir and Freundlich fitting were used in both sets of experiments. The Langmuir model (equation 5) was selected as it is the most common fitting, representing the maximum amount of molecules that can be adsorbed to form a complete monolayer coverage of the surface (Langmuir 1918; Mohammed et al. 2015). Meanwhile, The Freundlich model (equation 6) (Freundlich 1907) was selected as it better explains the adsorption

onto heterogeneous surfaces, with variations in the heat adsorption, and multilayer formation (Adamson and Gast 1997; Ali 2012; Lombardo and Thielemans 2019).

$$\frac{C_e}{q_e} = \frac{C_e}{q_{max}} + \frac{1}{k_L q_{max}} \quad (5)$$

$$Lnq_e = Lnk_F + \frac{1}{n} LnC_e \quad (6)$$

where C_e is the concentration of MB in the solution, k_L and k_F are the corresponding kinetic rates, and q_{max} is the maximum adsorption possible of the system tested.

3. Discussion and Results

3.1 Composite hydrogel bead formation

Bead shaped hydrogels were obtained from the starting nanocellulose alkaline solutions once they were dropped into the nitric acid coagulation bath. It was also possible to obtain beads when up to 50% of the total initial solid content of the solution was substituted with Tara gum. However, after 40% substitution a clear difference in the morphology of the beads was perceived, as the regeneration of the solutions resulted in less opaque beads with larger diameters. Beads resulting after 50% substitution were fragile and hard to manipulate, suggesting that optimum substitution of Tara gum is up to 40%.

When the solid content was evaluated, the pure cellulose nanofibril beads showed a solid content of 2.15 ± 0.08%, which increased to 2.72 ± 0.10% and 2.95 ± 0.24% when 10 and 30% of the initial mass was substituted with Tara gum, respectively. This

208 increase suggests that the formation of the beads occurred in the same way, with the
209 cellulose regenerating into fibrils during coagulation and the Tara gum attaching to the
210 surfaces of the formed fibers by hydrogen bonding, increasing the solid content of the
211 overall structure (Ma et al. 2016). Furthermore, with higher contents of Tara gum,
212 distinguishable phases can form and aggregates can be present (Ma et al. 2016). Still,
213 when 40% of the CNF was substituted, the average solid content suddenly dropped to
214 0.98±0.01%. Conversely, comparing the size of the beads made only with CNF and
215 those with 40% TG, the diameters were 2.8 ± 0.2 mm and 2.6 ± 0.1 mm, respectively.
216 Thus, the change in solid content, along with the small difference in size, but with a
217 clear difference in visual aspect, suggest that the presence of Tara gum as a structural
218 component affects the formation of the bead, probably allowing the Tara gum to act as
219 bridge between the cellulose nanofibrils as observed in other systems (Lopez-Sanchez
220 et al. 2015).

221 XRD spectra presented in Fig. 1a, confirmed the regeneration process of the CNF
222 for the formation of the beads, as the peaks observed in the CNF spheres correspond to
223 a cellulose II configuration (Gong et al. 2017). Conversely, the TG spectrum does not
224 present the typical peaks at 16.86° and 21.86°(Ma et al. 2016), instead, a different peak
225 is present at 15.4°; this new peak is likely due to the impurities of other components
226 present in TG that remain after extractions. Nevertheless, the composite material clearly
227 shows the signals from cellulose II. Additionally, the new peak observed in the TG
228 spectra confirms the incorporation of the TG into the bead structure.

229 FTIR-ATR spectra for all the generated beads, as well as for raw Tara gum powder
230 are provided in supplementary information (Fig. S1). Meanwhile, Fig. 1b shows the
231 spectra for pure CNF, pure TG, and composite beads generated with the best composite

generated, CNF-TG 60:40. For the TG spectrum, it would be expected to see bands relatable to mannose and galactose units. Instead, signals typical of asymmetrical carboxyl groups (ca. 1750 cm^{-1}) are clearly observed, attributed to protein and other lignocellulosic impurities remaining in the TG, and confirmed by the EA (Fig. 1c). Some of these carboxyl containing impurities do not seem to be regenerated with the polysaccharides, as it has been shown that lignin and tannin impurities depolymerize in the presence of urea/NaOH solution (Liu et al. 2020). Additionally, there is also a distinctive C-H bonds signal present, with a wider band at around 2900 cm^{-1} when the TG is compared to the pure CNF beads, this can also be relate to non-symmetrical H-bonding in the TG (Mondal et al. 2019). Also when comparing, there is a clear difference in the bands for CNF and TG related to the C-C and C-O-C signals of the ring are observed in the fingerprint area (<1400 cm^{-1}) (Prado et al. 2005).

Conversely, the differences between the pure CNF beads and the composite beads containing 40% of Tara gum are less noticeable at first glance. The main difference is observed at 1620 cm^{-1}, as the band's intensity is clearly reduced, suggesting less adsorbed water (Fan et al. 2012). On the contrary, the bands of the out of the plane O-H bending around 800 cm^{-1} increased, as evidence of the presence of TG in the beads. A slight change is also visible in the bands related to the C-O and C-C stretching (ca. 1164 to 1005 cm^{-1}), which had a hypsochromic shift as more α bonds are present. Similarly, at 1466cm^{-1}, a decrease in intensity of the band was observed when TG is added to CNF, which has been linked to the interaction between these two polymers and less freedom of the C-H bending due to non-conventional H-bonding (Mondal et al. 2019; Chen et al. 2020).

255 The EA (Fig. 1c) showed the increase of 0.04% nitrogen on the composite beads once
256 the TG was added, lowering the carbon content by 1.4% from the pure CNF beads.
257 Regarding the thermal properties (Figure 1d), the maximum degradation, shown by the
258 peak in the first derivative of the plot, was observed at 344 °C for TG. Meanwhile, there
259 was no difference between the CNF and CNF-TG beads after the substitution, with both
260 presenting it at 389 °C, which correspond to those values found in literature for
261 degradation of cellulose (380°C) (Larsson et al. 2013). However, the CNF had a sharp
262 peak when the first derivative was observed, while the CNF-TG presented a shoulder
263 before the maximum as observed on a Tara gum matrix reinforced with cellulosic
264 materials (Ma et al. 2016). However, the temperature point where thermal degradation
265 starts (onset T) decreased 4°C from 359°C for the CNF to 355°C for the CNF-TG
266 60:40.This increase could be related to the more porous structure and to a less
267 crystalline structure formed by the cellulose during regeneration due to the interference
268 of the Tara gum (Prasad et al. 2010), leading to a faster degradation, as well as being
269 closer to the onset temperature of Tara gum at 317 °C.
270
271 Fig. 1. Characterization of the CNF beads, CNF-TG 60:40 beads, and Tara gum. (a) XRD
272 spectra of both beads and Tara gum;(b) FTIR-ATR spectra of both beads and the Tara gum
273 powder; (c)elemental percentage content data from the EA of the samples; and (d)
274 thermogravimetric analysis with data extracts on the insert table.
275
276 The surface morphology of the beads was observed using SEM, the images obtained
277 (Fig. 2) confirms that the regeneration of the fibers is different in the presence of Tara
278 gum. Pure CNF beads (Fig. 2a) regenerate in wider fibers with a layered interior,

allowing for a smoother and more continuous surface. On the other hand, the composite beads containing TG (Fig. 2b) appeared to form thinner fibers that interlock forming a fiber network. This web-like structure is expected to contribute for a better water retention behavior due the increase of porous structures and the surface area (Cao et al., 2013).

Fig. 2. SEM images of (a) CNF beads and (b) CNF-TG 60:40 beads.

3.2 Methylene Blue adsorption

The efficiency of the beads with all the different substitution ratios of TG were tested for the removal of methylene blue; this information is presented in Fig. S2. As expected, an increase in the concentration of Tara gum in the composite beads improved the adsorption capacity of the hydrogel, as more surface area and functional groups (like amino groups and aldehydes) from the impurities on TG were introduced into the structure. Furthermore, there was a perceptible visual difference (Fig. S3) with the beads containing TG, as they presented spots of saturated color, suggesting a higher presence of TG in such area. This also serves as a visual confirmation of the presence of TG in the composite beads.

Likewise, the remotion of the dye was similar in the experiments done with the beads containing 30 and 40% of TG. Nevertheless, as the solid content of the beads was significantly different between them, with the 40% being lighter and therefore having a higher adsorption capacity, the focus was kept on the CNF-TG 60:40 beads (Fig. 3).

301 Pure CNF beads were able to remove 6.5% from a 15-ppm solution using only 5 beads
302 (8 mg wet weight, or 0.17 mg dry base), while in the case of composite CNF-TG 60:40
303 beads 9.9% was removed using the same number of beads (0.08 mg dry base). The
304 pseudo kinetics were calculated to better explain the behavior and calculate the
305 equilibrium adsorption (Table 1). The best fitting for both systems was into the pseudo-
306 second-order kinetic representing chemisorption and adsorption (Liu 2008). The CNF
307 derived beads presented a q_e of 62.11 mg/g, while the CNF-TG 60:40 had an adsorption
308 capacity of 200 mg/g. Despite the removal efficiency being lower than 10%, the
309 adsorption capacity obtained for the pure cellulose beads is comparable with data
310 reported in existing literature using regenerated cellulose as an adsorbent (Dai et al.
311 2021). Adsorption shown by composite beads at CNF-TG 60:40 ratio was higher than
312 the corresponding adsorption by pure cellulose beads.

313

314 Fig. 3. Results of the adsorption kinetic experiments of 5 beads of CNF and CNF-TG 60:40
315 beads in a 15-ppm methylene blue (MB) solution corresponding to (a) removal efficiency, (b)
316 adsorption capacity in mg of dye per gram of material, as well as the pseudo kinetic model fittings
317 for (c) pseudo-first-order, and (d) pseudo-second-order.

318

319 Table 1. Parameters for adsorption of methylene blue (MB) by the hydrogel beads.

Adsorption system	Pseudo-first order			Pseudo-second order		
	qe (mg/g)	k_1 (min^{-1})	R^2	qe (mg/g)	k_2 (g/mg min)	R^2
CNF	31.07	0.0026	0.8644	62.11	0.0002	0.9935
CNF-TG 60:40	95.13	0.0034	0.9201	200.0	0.0001	0.9971

320

321 It is worth considering that even if the same number of beads were placed, the solid
322 content was significantly lower in the beads containing Tara gum. Therefore, adsorption

323 isotherms were performed and experiments with a constant methylene blue
324 concentration and varying beads mass to better understand this phenomenon.

325 For the case of isotherms (Fig. 4), it can be observed that when the concentration is
326 increased up to 8-ppm, the adsorption increased with an almost linear trend in both,
327 neat CNF, and composite CNF-TG systems. The adsorption was similar in the case of
328 the isotherms at 8 and 10-ppm solutions, as they are statistically similar. An increase in
329 adsorption was observed when increasing the solution concentration to 10 and 15 ppm.
330 In all conditions, beads containing Tara gum presented the highest adsorption capacity,
331 even when both bead systems presented similar adsorption percentage. The obtained
332 data were fit into a Langmuir model (Table 2, Fig. 4c). The resulting modeling showed
333 that the maximum adsorption capacity of the CNF beads was of 8.28 mg/g with a kinetic
334 constant of 0.14 L/mg. Meanwhile, the CNF-TG 60:40 beads showed a higher
335 maximum adsorption of 13.7 mg/g but with a similar constant of 0.18 L/mg, suggesting
336 a similar adsorption mechanism for both systems (Tran et al. 2013; Bartczak et al.
337 2017). However, the maximum obtained was lower than what was obtained with the
338 kinetic model, showing a high impact in adsorption capacity depending on the sorbent
339 mass utilized. Likewise, as never-dried hydrogels were utilized, the adsorption
340 capacities presented herein account for both, adsorption on the fiber surface and
341 osmotic exchange between the beads and the media.

342 When Freundlich fitting was applied (Table 2, Fig. 4d), n >1 in both cases,
343 suggesting the formation of multilayers on the surface upon the dye adsorption (Kardam
344 et al. 2014; Wang et al. 2018). The different behavior can be attributed to the difference
345 on structure on the beads surface as observed with SEM and to the different functional
346 groups added with the TG (Fig. 2).

Fig. 4. (a) Adsorption capacity and (b) removal percent of the CNF and CNF-TG 60:40 beads obtained from the constant mass (200 wet mg) isotherm in solutions with 2, 5, 8, 10, and 15-ppm of methylene blue; (c) shows the Langmuir model fitting of the data, while (d) corresponds to the Freundlich model fitting.

Table 2. Isotherms model parameters for the adsorption of methylene blue onto CNF and CNF-TG 60:40 beads.

Sample	**Langmuir**			**Freundlich**		
	q_{max} [mg/g]	k_L [L/mg]	R^2	**n**	k_F [mg/g][L/mg]$^{1/n}$	R^2
CNF	8.28	0.14	0.93	1.68	4.51	0.94
CNF-TG 60:40	13.7	0.18	0.96	2.13	0.92	0.97

On the other hand, in the experiments with varying mass (Fig. 5) an almost linear response for the CNF beads up to 600 mg was observed, after which the adsorption capacity decreased. These results suggest that longer times might be needed for the saturation of the beads surface, than what was first observed in the kinetic and isotherm experiments. In the case of the CNF-TG 60:40 beads, a clear trend was not observed, but an overall decrease of adsorption capacity can be observed as the mass of sorbent increased.

When the removal efficiency is compared (Figure 5b), the CNF beads were able to remove around 60% of the methylene blue dye, which was 10% more than the composite CNF-TG beads. This is relevant as the removal efficiency is comparable among both types of beads, even when the beads containing Tara gum have 54% less dry mass on the structure. Another important observation is that when analyzing the exponential fitting of the percentage of adsorption, both systems showed similar trends, both with correlation coefficients (R) of 0.92. These trend lines were skewed mostly by the removal capacity of the last points 0.6 to 0.8 g for CNF and 0.7-0.8 g for CNF-TG 60:40, which seem to be close to the saturation capacity on both systems.

Fig. 5. (a) Adsorption capacity and (b) removal percent of the data obtained from isotherms varying the amount of sorbent -CNF and CNF-TG 60:40 beads- from 0.1 to 0.8 g on solutions with 15-ppm of methylene blue.

As expected, the interactions between the beads and the methylene blue increased with increasing contents of Tara gum present in the composite beads. This relates to the increase on functional groups on the Tara gum, which can then interact by electrostatic interactions with the methylene blue cationic groups (El Qada et al. 2006). Furthermore, the use of regenerated cellulose also provides cellulose with a planar surface (110) which is hydrophobic (Yamane et al., 2006); this surface would also drive the interaction with hydrophobic moieties on the pollutants (Lombardo and Thielemans 2019).

Likewise, as evidenced by the Freundlich fitting and the visual observation, the dye aggregates on the fibers surface, while also been entrapped in the hydrogel liquid phase.

The latter, induced by a difference of concentration between the water trapped in the beads structure and the water present in the outside media. Furthermore, the lower solid content of the CNF-TG 60:40 did not prevent the structure to form and perform similarly to the pure CNF beads. With a removal of around 50% of the dye from a 15-ppm was achieved with only 8 mg of wet mass. This opens the possibility of generating adsorbent for water treatment utilizing up to 40% of low-cost, alternative carbohydrates.

Conclusions

In this work, we were able to generate cellulose beads from cellulose nanofibril, instead of traditional pretreated mill pulp, diversifying the raw materials when using alternative sources such as by-products from other agro-industrial operations (Gómez-Maldonado et al. 2020). Furthermore, we demonstrated that up to 40% of the cellulose can be substituted for other carbohydrates (*i.e.*, Tara gum).

When the beads were tested to adsorb commonly discarded dyes such as methylene blue, it was observed that the beads containing Tara gum had improved adsorption by 39.6% in the isotherm experiments. Furthermore, when the sorbent concentration was varied, this improved 38% was maintained, suggesting that the best performance will be sustained independently of the conditions.

Thus, this work demonstrated that innovative sorbents for water treatment can be generated using diverse lignocellulosic materials, seizing not only the cellulose nanofibrils but also gums used nowadays for low-end products. Furthermore, using Tara gum could also decrease the price of cellulose-based adsorbents, as gums have a

lower production cost while still being highly available. Therefore, the substitution of a high percentage of the solid mass for these gums will result in a cheaper alternative for water treatment.

Acknowledgments

This work was supported by the USDA National Institute of Food and Agriculture, Hatch program (ALA013-17003), and McIntire-Stennis program (1022526). The School of Forestry and Wildlife Sciences at Auburn University's financial support to complete this work is much appreciated. The authors also want to acknowledge the Fondo Nacional de Desarrollo Científico, Tecnológico y de Innovación Tecnológica Prociencia, through project N° 09-2020-FONDECYT-BM and to the Instituto de Investigación Científica (IDIC) of Universidad de Lima for their financial support for the research stay. The Bioenergy Center of Auburn University for the access to their thermogravimetric analyzer.

Declarations

Conflict of Interest. The authors declare no conflict of interest.

Data Availability. Data is available upon reasonable request to authors.

References

AdamsonAdamson AW, Gast AP (1997) Physical Chemistry of Surfaces, Sixth Edition. Wiley-Interscience publication

Ali I (2012) New generation adsorbents for water treatment. Chem Rev 112:5073–

5091. https://doi.org/10.1021/cr300133d

Bartczak P, Klapiszewski Ł, Wysokowski M, et al (2017) Treatment of model solutions and wastewater containing selected hazardous metal ions using a chitin/lignin hybrid material as an effective sorbent. J Environ Manage 204:300–310. https://doi.org/10.1016/j.jenvman.2017.08.059

Cai Z, Sun Y, Liu W, et al (2017) An overview of nanomaterials applied for removing dyes from wastewater. Environ Sci Pollut Res 24:15882–15904. https://doi.org/10.1007/s11356-017-9003-8

Chen Y, Xu L, Wang Y, et al (2020) Characterization and functional properties of a pectin/tara gum based edible film with ellagitannins from the unripe fruits of Rubus chingii Hu. Food Chem 325:126964. https://doi.org/10.1016/j.foodchem.2020.126964

Dai H, Chen Y, Ma L, et al (2021) Direct regeneration of hydrogels based on lemon peel and its isolated microcrystalline cellulose: Characterization and application for methylene blue adsorption. Int J Biol Macromol 191:129–138. https://doi.org/10.1016/j.ijbiomac.2021.09.063

El Qada EN, Allen SJ, Walker GM (2006) Adsorption of Methylene Blue onto activated carbon produced from steam activated bituminous coal: A study of equilibrium adsorption isotherm. Chem Eng J 124:103–110. https://doi.org/10.1016/j.cej.2006.08.015

Fan M, Dai D, Huang B (2012) Fourier Transform Infrared Spectroscopy for Natural Fibres. Fourier Transform - Mater Anal. https://doi.org/10.5772/35482

Forgacs E, Cserháti T, Oros G (2004) Removal of synthetic dyes from wastewaters: A review. Environ Int 30:953–971. https://doi.org/10.1016/j.envint.2004.02.001

Freundlich H (1907) Über die Adsorption in Lösungen. Zeitschrift für Phys Chemie 57U:385–470. https://doi.org/10.1515/zpch-1907-5723

Gomez-Maldonado D, Filpponen I, Johansson LS, et al (2021a) Environmentally dependent adsorption of 2,4-dichlorophenol on cellulose-chitosan self-assembled composites. Biopolymers. https://doi.org/10.1002/bip.23434

Gómez-Maldonado D, Hernández-Guerrero M, López-Simeon R, et al (2020) Lignocellulosic-Derived Nanostructures From Latin American Natural Resources: Extraction, Preparation, and Applications. In: Lignocellulosics. Elsevier, pp 91–115

Gomez-Maldonado D, Reynolds AM, Johansson L-S, et al (2021b) Fabrication of aerogels from cellulose nanofibril grafted with β-cyclodextrin for capture of water pollutants. J Porous Mater 28:1725–1736. https://doi.org/10.1007/s10934-021-01109-w

Gong J, Li J, Xu J, et al (2017) Research on cellulose nanocrystals produced from cellulose sources with various polymorphs. RSC Adv 7:33486–33493. https://doi.org/10.1039/c7ra06222b

Gürses A, Açıkyıldız M, Güneş K, Gürses MS (2016) Classification of dye and pigments. In: Dyes and Pigments. Springer, pp 31–45

Jonoobi M, Oladi R, Davoudpour Y, et al (2015) Different preparation methods and properties of nanostructured cellulose from various natural resources and residues: a review. Cellulose 22:935–969. https://doi.org/10.1007/s10570-015-0551-0

Kardam A, Raj KR, Srivastava S, Srivastava MM (2014) Nanocellulose fibers for biosorption of cadmium, nickel, and lead ions from aqueous solution. Clean

Technol Environ Policy 16:385–393. https://doi.org/10.1007/s10098-013-0634-2

Klemm D, Kramer F, Moritz S, et al (2011) Nanocelluloses: A new family of nature-based materials. Angew Chemie - Int Ed 50:5438–5466. https://doi.org/10.1002/anie.201001273

Lang AR (2009) Dyes and Pigments: New Research. Nova Science Publishers

Langmuir I (1918) The adsorption of gases on plane surfaces of glass, mica and platinum. J Amer 40:1361–1403

Larsson E, Sanchez CC, Porsch C, et al (2013) Thermo-responsive nanofibrillated cellulose by polyelectrolyte adsorption. Eur Polym J 49:2689–2696. https://doi.org/10.1016/j.eurpolymj.2013.05.023

Liu J, Wang L, Li J, et al (2020) Degradation mechanism of Acacia mangium tannin in NaOH/urea aqueous solution and application of degradation products in phenolic adhesives. Int J Adhes Adhes 98:102556. https://doi.org/10.1016/j.ijadhadh.2020.102556

Liu Y (2008) New insights into pseudo-second-order kinetic equation for adsorption. Colloids Surfaces A Physicochem Eng Asp 320:275–278. https://doi.org/10.1016/j.colsurfa.2008.01.032

Lombardo S, Thielemans W (2019) Thermodynamics of adsorption on nanocellulose surfaces. Cellulose 26:249–279. https://doi.org/10.1007/s10570-018-02239-2

Long LY, Weng YX, Wang YZ (2018) Cellulose aerogels: Synthesis, applications, and prospects. Polymers (Basel) 8:1–28. https://doi.org/10.3390/polym10060623

Lopez-Sanchez P, Schuster E, Wang D, et al (2015) Diffusion of macromolecules in self-assembled cellulose/hemicellulose hydrogels. Soft Matter 11:4002–4010.

https://doi.org/10.1039/c5sm00103j

Luan Q, Zhang H, Lei Y, et al (2021) Microporous regenerated cellulose-based macrogels for covalent immobilization of enzymes. Cellulose 28:5735–5744. https://doi.org/10.1007/s10570-021-03887-7

Ma Q, Hu D, Wang L (2016) Preparation and physical properties of tara gum film reinforced with cellulose nanocrystals. Int J Biol Macromol 86:606–612. https://doi.org/10.1016/j.ijbiomac.2016.01.104

Ma Q, Wang L (2016) Preparation of a visual pH-sensing film based on tara gum incorporating cellulose and extracts from grape skins. Sensors Actuators, B Chem 235:401–407. https://doi.org/10.1016/j.snb.2016.05.107

Mahmoud HR, El-Molla SA, Saif M (2013) Improvement of physicochemical properties of Fe2O3/MgO nanomaterials by hydrothermal treatment for dye removal from industrial wastewater. Powder Technol 249:225–233. https://doi.org/10.1016/j.powtec.2013.08.021

Mohammed N, Grishkewich N, Berry RM, Tam KC (2015) Cellulose nanocrystal–alginate hydrogel beads as novel adsorbents for organic dyes in aqueous solutions. Cellulose 22:3725–3738. https://doi.org/10.1007/s10570-015-0747-3

Mokhtar A, Abdelkrim S, Djelad A, et al (2020) Adsorption behavior of cationic and anionic dyes on magadiite-chitosan composite beads. Carbohydr Polym 229:115399. https://doi.org/10.1016/j.carbpol.2019.115399

Mondal H, Karmakar M, Chattopadhyay PK, Singha NR (2019) Starch-g-tetrapolymer hydrogel via in situ attached monomers for removals of Bi(III) and/or Hg(II) and dye(s): RSM-based optimization. Carbohydr Polym 213:428–440. https://doi.org/10.1016/j.carbpol.2019.02.035

Ponce S, Chavarria M, Norabuena F, et al (2020) Cellulose Microfibres Obtained from Agro-Industrial Tara Waste for Dye Adsorption in Water. Water Air Soil Pollut 231:. https://doi.org/10.1007/s11270-020-04889-0

Prado BM, Kim S, Özen BF, Mauer LJ (2005) Differentiation of carbohydrate gums and mixtures using fourier transform infrared spectroscopy and chemometrics. J Agric Food Chem 53:2823–2829. https://doi.org/10.1021/jf0485537

Prasad K, Mine S, Kaneko Y, Kadokawa JI (2010) Preparation of cellulose-based ionic porous material compatibilized with polymeric ionic liquid. Polym Bull 64:341–349. https://doi.org/10.1007/s00289-009-0144-x

Qiu X, Hu S (2013) "Smart" materials based on cellulose: A review of the preparations, properties, and applications. Materials (Basel) 6:738–781. https://doi.org/10.3390/ma6030738

Rahimian R, Zarinabadi S (2020) A review of Studies on the Removal of Methylene Blue Dye from Industrial Wastewater Using Activated Carbon Adsorbents Made from Almond Bark. Prog Chem Biochem Res J homepage 3:251–268

Ruan C, Strømme M, Lindh J (2016) A green and simple method for preparation of an efficient palladium adsorbent based on cysteine functionalized 2,3-dialdehyde cellulose. Cellulose 23:2627–2638. https://doi.org/10.1007/s10570-016-0976-0

Ruan CQ, Strømme M, Lindh J (2018) Preparation of porous 2,3-dialdehyde cellulose beads crosslinked with chitosan and their application in adsorption of Congo red dye. Carbohydr Polym 181:200–207. https://doi.org/10.1016/j.carbpol.2017.10.072

Shore J (2002) Colorants and auxiliaries : organic chemistry and application properties. Society of Dyers and Colourists

Tran CD, Duri S, Delneri A, Franko M (2013) Chitosan-cellulose composite materials : Preparation , Characterization and application for removal of microcystin. J Hazard Mater 253:355–366

Trygg J, Fardim P (2011) Enhancement of cellulose dissolution in water-based solvent via ethanol-hydrochloric acid pretreatment. Cellulose 18:987–994. https://doi.org/10.1007/s10570-011-9550-y

Trygg J, Fardim P, Gericke M, et al (2013) Physicochemical design of the morphology and ultrastructure of cellulose beads. Carbohydr Polym 93:291–299. https://doi.org/10.1016/j.carbpol.2012.03.085

Trygg J, Yildir E, Kolakovic R, et al (2015) Solid-state properties and controlled release of ranitidine hydrochloride from tailored oxidised cellulose beads. Macromol Mater Eng 300:210–217. https://doi.org/10.1002/mame.201400175

Trygg J, Yildir E, Kolakovic R, et al (2014) Anionic cellulose beads for drug encapsulation and release. Cellulose 21:1945–1955. https://doi.org/10.1007/s10570-014-0253-z

Wang DM, Hao G, Shi QH, Sun Y (2007) Fabrication and characterization of superporous cellulose bead for high-speed protein chromatography. J Chromatogr A 1146:32–40. https://doi.org/10.1016/j.chroma.2007.01.089

Wang J, Wei L, Ma Y, et al (2013) Collagen/cellulose hydrogel beads reconstituted from ionic liquid solution for Cu(II) adsorption. Carbohydr Polym 98:736–743. https://doi.org/10.1016/j.carbpol.2013.06.001

Wang X, Jiang C, Hou B, et al (2018) Carbon composite lignin-based adsorbents for the adsorption of dyes. Chemosphere 206:587–596. https://doi.org/10.1016/j.chemosphere.2018.04.183

Wu Y, Ding W, Jia L, He Q (2015) The rheological properties of tara gum (Caesalpinia spinosa). Food Chem 168:366–371. https://doi.org/10.1016/j.foodchem.2014.07.083

Zhang L, Zhou J, Zhang L (2013) Structure and properties of β-cyclodextrin/cellulose hydrogels prepared in NaOH/urea aqueous solution. Carbohydr Polym 94:386–393. https://doi.org/10.1016/j.carbpol.2012.12.077

580 **Supplementary information**

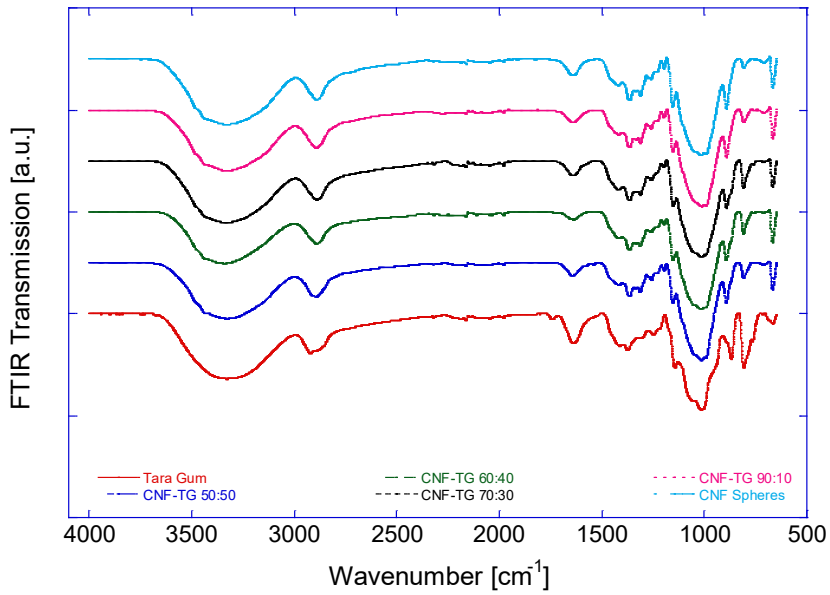

Fig. S1. FTIR-ATR spectra of Tara gum, CNF beads, and beads containing 10, 30, 40 or 50% Tara gum.

585

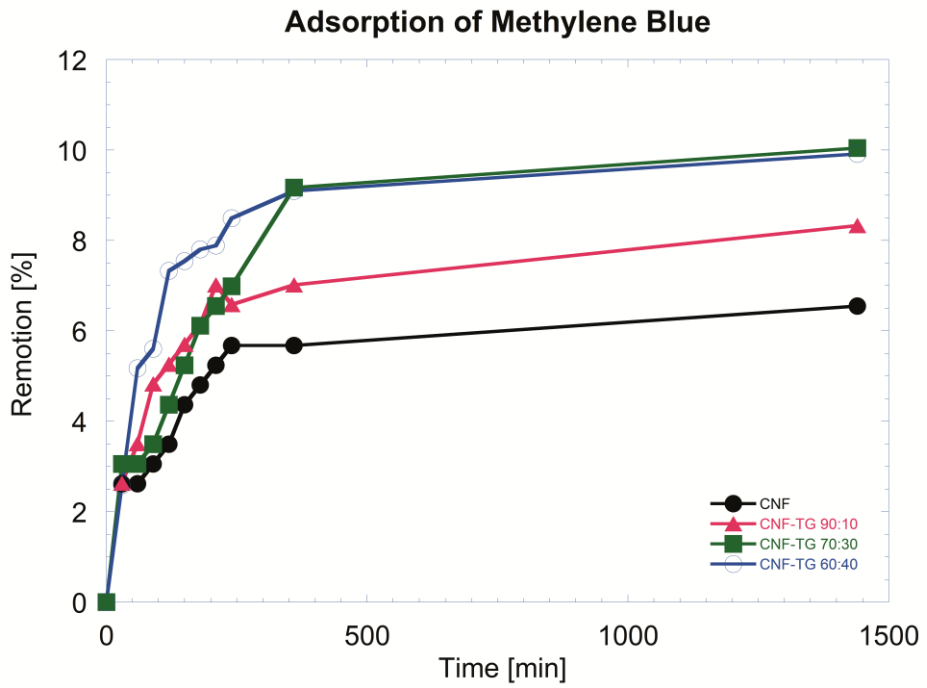

Fig. S2. Removal capacity of the CNF beads, and beads containing 10, 30 or 40% Tara gum. Removal is expressed in percentage; the experiments were done with 5 beads of each material in a 15-ppm methylene blue solution.

590

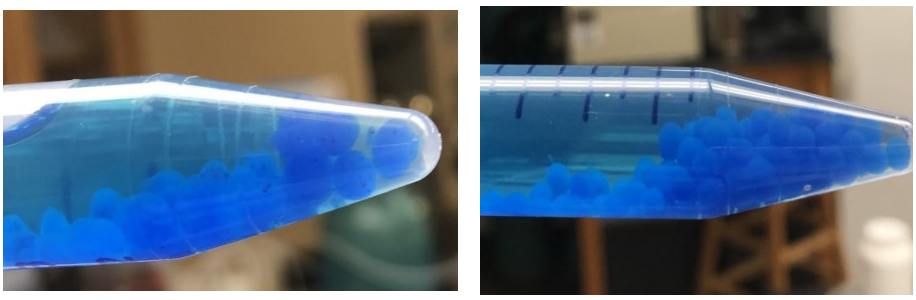

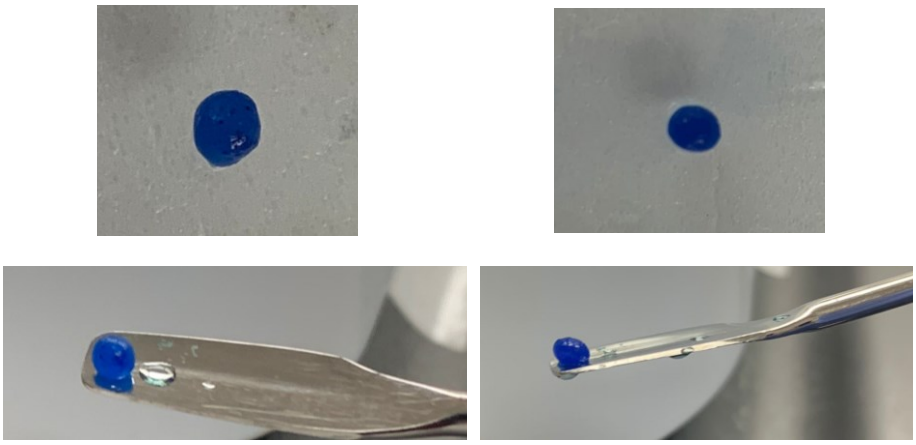

(a) (b)

Fig. S3. Picture of the (a) CNF-TG 60:40 and (b) CNF after adsorption of methylene blue